Intensification of liquid-liquid emulsification process in a rotating solid foam stirrer tank: experiments and modeling

Ze-Teng Wang [1], Si-Xing Chen [1], Yi Ouyang [2], Xue-Qin Zhang [1], Bing-De Zheng [1],

Na Zhang [1], Jing Ye [1], Mei-Tian Xiao [1], Yu-Cheng Yang [1*]

1. Department of Chemical and Pharmaceutical Engineering, School of Chemical Engineering, Huaqiao University, Xiamen, Fujian, P.R. China, 361021

2. Laboratory for Chemical Technology, Ghent University, Technologiepark, Gent, Belgium, 125, 9052

Abstract

Process intensification equipment is playing an increasingly role in emulsion process. A novel rotating solid foam stirrer tank (RSFST) is developed in this work to try to intensify liquid-liquid emulsification process. The effects of operating parameters and physical parameters (emulsification time, rotational speed, packing size, dispersed phase volume fraction and continuous-phase viscosity) on the droplet size distribution (DSD) and Sauter mean diameter d_{32} of oil-in-water emulsions produced in RSFST were investigated using kerosene-water as the system. To benchmark the emulsion performance of the RSFST, the Rushton (RT) stirrer is used a reference stirrer and the generated droplet size and average energy dissipation rate as evaluation metrics. Based on the experiment data of emulsification under different operating conditions and physical parameters, models are applied to describe the bimodal distribution of oil-in-water emulsions droplet size, and correlation is proposed to predict the Sauter mean

diameter d_{32} of RSFST. This work provides fundamental data for practical application of RSFST used in emulsion process intensification.

1. Introduction

Emulsification of two immiscible liquids is an important unit operation in the chemical, petroleum and food industries[1]. From the perspective of its fundamentals, droplet size distribution plays an important role in the emulsion process and has a significant impact on heat and mass transfer efficiency[2]. In general, the emulsions are formed by the dynamic equilibrium of droplet coalescence and breakup. The former mainly leads to the formation of a larger drop from two or more smaller drops, and the latter leads to the formation of smaller drops from a larger one. The commonly used emulsifying equipment in industry is a flat blade or curved blade turbine agitator[3]. The flat blade has high shear force and turbulent diffusion capacity, which is especially suitable for shear dispersion operation. The curved blade belonging to the straight blade, and because of its special backward curved structure, it has better discharge performance and is suitable for emulsification operation. Although the equipment are easy to operate and mature technology, it is hard to provide higher energy to produce small dispersed phase droplets smaller, and only the energy dissipation rate near the stirrer is high, resulting in low equipment efficiency [4]. With the development of process intensification equipment, some intensified emulsifying equipment [5], such as high-shear mixer, high-pressure homogenizer and ultrasonic emulsifier have been widely studied [6]. High-shear mixer is a new type of process intensification device, which uses mechanical rotation at high speed so that the material is subjected to strong shearing in the stator-rotor gap to obtain emulsions with smaller droplet size [7]. However, its high energy consumption of the motor and complex geometric structure hinders its application. High-pressure homogenizers operate at high pressures of 10-40 Mpa to obtain extremely high velocities of the dispersed phase. After passing through the orifices, the droplets are crushed into tiny droplets by the dual effects of expansion by loss of pressure and impact collision at high speed [8]. The pressurization process is energy intensive as well. Ultrasonic emulsification equipment crushes and disperses droplet by the cavitation effect of ultrasound, which can quickly generate emulsions with smaller droplet size [9]. However, it has the weakness of low processing capacity. Equipment with low energy consumption, large processing capacity and the ability to generate fine droplets are the targeted characteristics for liquid-liquid emulsification.

A RSFST is a novel type of a multi-phase stirred tank equipped with a porous ceramic packing instead of the traditional stirring paddles [10]. The key feature of an RSFST is that a strong centrifugal force and shear force are induced simultaneously from the mechanical rotation of the porous foam packing, which shows a strong ability to intensify gas-liquid contact and increase interfacial area. In recent years, the reactor has demonstrated advantages in gas-liquid processes such as catalytic oxidation of glucose[11], catalytic hydrogenation of styrene[12], mass transfer of ozone and degradation of acidic red B by foam packed loaded catalyst in semi-intermittent operation[13], degradation of acidic red B and *p*-nitrophenol by ozone in continuous operation[14], micro-mixing efficiency[15] and liquid-solid mass transfer[16]. Moreover, the corporation of Spin Chem AB developed the similar RSFST with 300-2000 mL reaction volume to intensify the bio-catalytic reaction process[14]. Previous research showed that due to the special structure of the stirrer in RSFST, it has good mixing efficiency, large processing capacity, low energy consumption and the ability to produce fine dispersed phase. However, the porous structure of the stirrer makes the flow pattern in RSFST more complex, resulting in the lack of certain theoretical support for its application. For the targeted application in this study, i.e. emulsification process intensification, the RSFST can bring benefits.

To the best of our knowledge, there are no reports on the study of liquid-liquid emulsification in this kind of stirred tank design. Therefore, in this work, a systematic experimental study is conducted to study the effects of operating conditions and physical parameters (emulsification time, rotational speed, packing size, dispersed phase volume fraction and continuous-phase viscosity) on droplet size distribution and Sauter mean diameter. The performance of RSFST as well as the energetic efficiency is evaluated by comparing it with Rushton agitator as a reference.

2. Theoretical background

2.1 Mechanistic models

According to different operating conditions and parameters, different models and theories are proposed to predict the size of droplets in emulsifying equipment[17]. It is generally believed that in turbulent flow, droplets can be broken by inertial stress or viscous stress, which depends on the size of droplets and the length scale of the smallest eddies η_k[18]. According to Kolmogorov' s theory[19], the length scale of the smallest eddies η_k depends on the energy dissipation rate and kinematic viscosity

$$\eta_k = \left(\frac{v_c^3}{\varepsilon}\right)^{\frac{1}{4}} \tag{1}$$

where v_c is the kinematic viscosity of the continuous phase and ε is the local energy dissipation rate.

When the inertial stress is greater than the interfacial tension stress in droplets breaking up process, the largest drop size in turbulent flow could be estimated by Kolmogorov′s local isotropy theory[20]. The maximum drop size (d_{max}) is correlated to dimensionless Weber number[21, 22].

$$\frac{d_{max}}{D} = C_1 We^{-0.6} \tag{2}$$

where *D* is the impeller diameter, C_1 is the dimensionless constant and *We* is the dimensionless Weber number. The Weber number shows the turbulence intensity and the physicochemical properties of the system[23].

$$We = \frac{\rho_c N^2 D^3}{\sigma} \tag{3}$$

where ρ_c is the density of the continuous phase, *N* is the impeller speed and σ is the interfacial tension.

Sprow[24] proposed that the Sauter mean diameter d_{32} are proportional to maximum stable droplet diameter d_{max}

$$d_{32} = C_2 d_{max} \tag{4}$$

Where the Sauter mean diameter d_{32} is

$$d_{32} = \frac{\sum_{i=1} f_n(d_i) d_i^3}{\sum_{i=1} f_n(d_i) d_i^2} = \frac{\sum_{i=1} f_v(d_i)}{\sum_{i=1} \frac{f_v(d_i)}{d_i}} \tag{5}$$

$$d_{32} = \frac{6\Phi}{a} \tag{6}$$

In the above equations, d_i is the ith droplet diameter, $f_n(d_i)$ is the frequency by number of the droplets of the *i*th diameter, $f_v(d_i)$ is the frequency by volume of the droplets of the *i*th diameter and a is the interface area per unit volume.

Eq. (4) makes d_{max} and d_{32} interchangable and has been widely used with several values for C_2 being reported in literature, e.g. C_2=0.45 in the study of Nishikawa et al.'s work[25], $C_2 = 0.16$ in a study of a rotor-stator mixer[26] are found. As such, d_{max} is replaced by d_{32} in **Eq. (2)**

$$\frac{d_{32}}{D} = C_3 We^{-0.6} \tag{7}$$

where C_3 is the dimensionless constant obtained experimentally depending on the tank geometry and impeller type[21].

The effect of the dispersed phase volume fraction Φ can be accounted by the modification of mechanistic models with a function of Φ, when the dispersion is well stabilized against coalescence and the rheological behavior does not alter[27].

$$\frac{d_{32}}{D} = C_4(1 + C_5\Phi)We^{-0.6} \tag{8}$$

where C_4 and C_5 depend on the impeller type and the coalescence tendency respectively. High values of C_5 represent a tendency of droplets to coalesce easily[28]. The values of C_5 vary between 0.5 and 20[1, 29].

According to Stamatoudis and Tavlarides[30] the following phenomenological models of drop breakage and coalescence functions was proposed for liquid-liquid dispersion in stirred vessels.

breakage rate of droplets of diameter *d*

$$\mathrm{r}_b'(d) = C_6 N(t) A'(d) exp\left(-\frac{C_7\sigma}{\mu_c^{-m}\rho_c^{m+1}N^{m+2}dD^{2m+3}T^2}\right) \tag{9}$$

coalescence frequency of droplets

$$F'(d,d') = C_8 N^2(t) A'^2(d) d^3 \left(\frac{\rho_c^{m+1}N^{m+3}}{\mu_c^{m+1}}\right)^{1/2} exp\left(-\frac{C_9 N D^2}{T^2}\right) D^{(2m+5)/2} \tag{10}$$

where $N(t)$ is total number of droplets at time *t* per unit dispersion volume, $A'(d)$ is the fraction of droplets with diameter *d*, T is the tank diameter, *m* is the slope of the log-log plot of impeller power vs. impeller Reynold's number.

2.2 Droplet size distribution

The polydispersity of the DSD is another important characteristic of the dispersion system. In general, three types of the distribution can be found in literature: normal distribution, log-normal distribution and Fréchet distribution.

Chen and Middleman[31] fitted a normal distribution to their DSD by volume.

$$P_v(d_i) = \frac{1}{\sqrt{2\pi}\sigma_d}\exp\left[-\frac{(d_i-\bar{d}_i)^2}{2\sigma_d^2}\right] \tag{11}$$

where $P_v(d_i)$ is the probability density function for droplet size distribution by volume, $\bar{d}_i$ is the mean diameter in the normal distribution, and σ_d is the respective standard deviation.

Hall et al.[32] and Chatzi et al.[33] found that for a bimodal distribution, **Eq. (11)** fails to describe the bimodal volume distribution due to the innate properties of the function.

Arai et al.[34] and Vankova et al.[35] found that log-normal distribution can better describe bimodal distributions by number.

$$P_n(d_i) = \frac{1}{d_i\sqrt{2\pi}\sigma_{\ln(d)}}\exp\left[-\frac{\left(\ln(d_i)-\overline{\ln(d_i)}\right)^2}{2\sigma_{\ln(d)}^2}\right] \tag{12}$$

where $\overline{\ln(d_i)}$ is the mean of $\ln(d_i)$ and $\sigma_{\ln(d)}$ its standard deviation.

Liu et al.[36] emulsified 9.6×10^{-3}-426×10^{-3} Pa·s viscosity range crude oils in water using a rotor–stator at different *N* and obtained bimodal DSDs. They transformed the DSD by volume into a number distribution (see **Eq. (13)**). This conversion resulted in a monomodal DSD by number. They further used three different probability density functions to fit the DSD by number; namely a normal, a lognormal and a Fréchet distribution. The results show that the Frechet distribution function fits the experimental data well.

$$f_n(d_i) = \frac{\frac{fv(d_i)}{d_i^3}}{\sum \frac{fv(d_i)}{d_i^3}} \tag{13}$$

$$P_n(d_i) = \frac{\alpha}{\beta}\left(\frac{\beta}{d_i}\right)^{\alpha+1} exp\left[-\left(\frac{\beta}{d_i}\right)^{\alpha}\right] \tag{14}$$

where α and β are obtained using the equations below

$$\beta^{\alpha} = \frac{n}{\sum_{i=1}^{n}\frac{1}{d_i^{\alpha}}} \tag{15}$$

$$\frac{n}{\alpha} + n\ln\beta - \sum_{i=1}^{n}\ln d_i - \sum_{i=1}^{n}\left(\frac{\beta}{d_i}\right)^{\alpha}\ln\left(\frac{\beta}{d_i}\right) = 0 \tag{16}$$

In this work, based on the above models, the DSD by number is described by normal distribution, log-normal distribution and Frechet distribution, and the linear relationship between Sauter mean diameter d_{32} and maximum stable droplet diameter d_{max} in bimodal volume DSD is studied. Finally, d_{32} was correlated using a modified model by considering the influence of the dispersed phase volume fraction on the droplet size.

3. Materials and methods

3.1 Materials and reagents

Distilled water and aqueous solutions of glycerin (gly#w) (Sinopharm Chemical Reagent Co., Ltd.) were used as the continuous phase. Kerosene (Aladdin reagent (Shanghai) Co., Ltd) is used as the dispersed phase. Tween 80 (Sinopharm Chemical

Reagent Co., Ltd.) was added to the continuous phase as an emulsifier to avoid coalescence of the dispersed phase. The critical micelle concentration of Tween 80, reported to be about 0.0013 wt%[37], is less than the concentration of Tween 80 used in the present work (0.0025 wt %). The densities of all fluids were measured by the pycnometer method. A rheometer (MCR-302, Shanghai antonpaar Trading Co., Ltd) was used for measuring the viscosities of the continuous phase and the dispersed phase. The interfacial tensions between the oils and the continuous phases were measured using an automatic surface tensiometer (SFZL-E1, Beijing Pin Zhi Xin Precision Instrument CO., Ltd). Results are shown in **Table 1**.

Table 1. Physical properties of all fluids investigated at 25°C

dispersed phase	continuous phase	μ_c (mPa·s)	ρ_c (kg/m^3)	μ_d (mPa·s)	ρ_d (kg/m^3)	σ (mN/m)
kerosene	water	1.3	1002.4	1.4	811.2	9.9
kerosene	(20 w/w) gly#w	1.8	1050.4	1.4	811.2	9.7
kerosene	(30 w/w) gly#w	2.6	1088.4	1.4	811.2	9.5
kerosene	(40 w/w) gly#w	3.1	1115.8	1.4	811.2	9
kerosene	(50 w/w) gly#w	5.1	1127.8	1.4	811.2	7.8

3.2 Experimental equipment

Figure 1(a) shows a schematic structure of the RSFST used in this study. A foam packing material is used as the stirrer. The packing is discharged into a circular block with a height (h) of 5 cm, an inner diameter (D_i) of 5 cm, and a outer diameter (D_o) with four different sizes (15, 13, 11 and 9 cm). It is made of Al_2O_3 hydrophobic material with a porosity of 0.88 and an average pore size of 0.09 cm (pore density 20 ppi), manufactured by Shanghai Precision Industrial Ceramics Co. The stirrer is installed in a transparent PMMA tank of diameter T=20 cm and height H=20 cm. The distance between the bottom of the foam packing and the tank bottom (C) is 3 cm. The tank inner wall and lid are equipped with four baffles of 1 cm thickness and width (B). The liquid inlet is located 8 cm from the center of the cover. Sampling port is installed at the center of the tank bottom. Meanwhile, **Figure 1(b)** shows a schematic structure of the Rushton stirrer (RT), a 6-blade stirrer with a diameter (D') of 7 cm and a blade size (l×w) of 1.75 × 1.4 cm. It is made of stainless steel as a reference stirrer for the comparison study. It is equipped in the same size of the tank, but the distance to the tank bottom (C') is 6.7 cm.

The energy consumptions of two stirred tank are calculated based on the applied torque measured by a torque sensor (Beijing Zrn Instrument Technology Co., Ltd). The power consumption is expressed as

$$P_{in} = 2\pi NM - 2\pi NM_n \tag{17}$$

where P_{in} is the power consumption (W), M is the torque (N·m), and M_n is the torque (N·m) of the bearing loss correction, measured using water and no impeller attached.

In order to compare the two impellers, the performance of two stirred tank are evaluated based on the estimated average energy dissipation rate. The average energy dissipation rate ε_{avg} can be calculated from the power input P_{in}:[38]

$$\varepsilon_{avg} = \frac{P_{in}}{\rho_c V_H} \tag{18}$$

where V_H is the working liquid volumes (L).

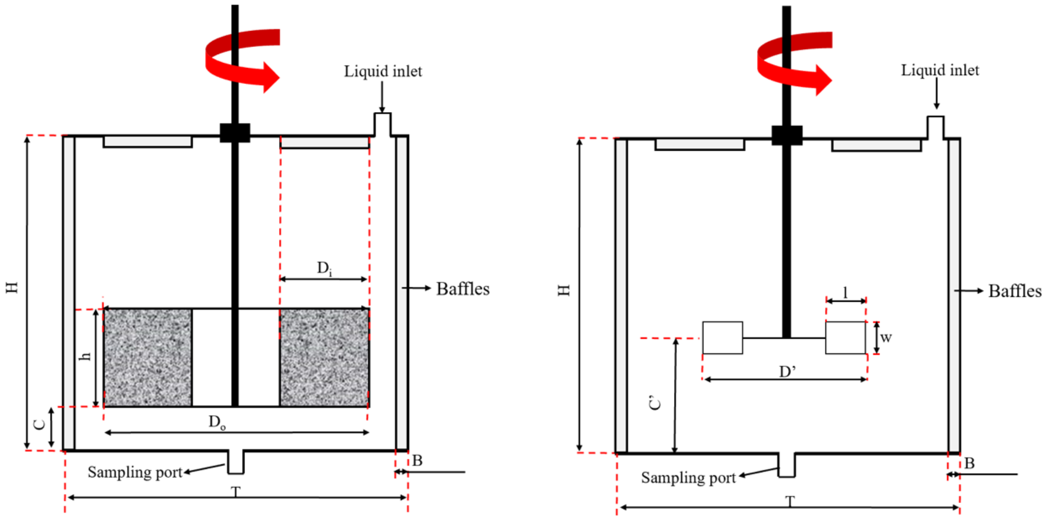

(a) (b)

Figure. 1. Schematic structurers of (a) RSFST and (b) RT stirrer

3.3 Experimental procedure

The operating conditions are shown in **Table 2**. The surfactant solution was prepared by charging the vessel with distilled water and then the required amount of Tween 80. A rotational speed of 100 rpm was used to ensure a well-mixed condition. After a short period of agitation, the required amount of oil was added into the top surface of the mixture of water and surfactant. Once this was completed high speed stirrer was switched on and the timer started. A sample of 30 ml of the emulsion was collected at the sampling point. The sample was then taken to the NKT6100-C wet laser particle sizer (Shandong NKT analysis instrument Co., Ltd) to measure the droplet size distribution. Each sample was analyzed three times. The experiment was repeated three times under the same operating conditions, and the average error was no more than 5%.

Table 2. Operating conditions

Items	Values
Rotational speed (rpm)	200, 250, 300, 350
Packing size (cm)	9, 11, 13, 15
Dispersed phase volume fraction (%)	0.75, 2, 3, 5
Continuous-phase viscosity (mPa·s)	1.3, 1.8, 2.6, 3.1, 5.1
Emulsification time (min)	10, 20, 30, 40, 50, 60, 70, 80
Working liquid volumes (L)	4

4. Results and discussion

4.1 Droplet diameter distribution and Sauter mean diameter d_{32}

4.1.1 Effect of emulsification time

The droplet diameter distribution of kerosene-water emulsion is shown in **Figure 2(a)**. The droplet diameter distribution of emulsion shows the form of bimodal droplet size distribution (DSDs). The changes of D_{10}, D_{50} and D_{90} values in the volume distribution with emulsification time are shown in **supplementary material Table 1S**. With the increase of emulsification time, the droplet diameter distribution shifted to the smaller droplet direction, and the proportion of small droplet peak increased. **Figure 2(b)** shows that the Sauter mean diameter d_{32} decreases with the increase of emulsification time and higher agitation speed can significantly decrease the d_{32}. The droplet breakup is related to the energy input provided by RSFST. At the beginning, it is relatively easy to brake the big oil droplets and the droplet diameter decreases obviously.

With the continuous reduction of the diameter of the oil droplets, more energy is required for further fragmentation, thus the tendency of the Sauter mean diameter d_{32}

decreasing with the emulsification time will gradually slow down until the equilibrium between the fragmentation and coalescence is reached. The experimental data, shown in **Figure 2(b)** as the solid points, is then fitted to an exponential first order equation [39], shown in **Figure 2(b)** as the solid lines. The lowest regression value of the fitting is 0.99. This equation gives an indication of the approach to the equilibrium Sauter mean diameter d_{32} and allows estimating the equilibrium value [39]. It can be seen from **Figure 2(b)** that the larger the rotational speed, the shorter the balancing time. This is because the higher the rotational speed, the stronger the shear effect, and the liquid is broken into smaller droplets, which increases the surface area of the liquid in oil-water two-phase contact and promotes the emulsification process. It can be seen from **Figure 2(b)** that the larger the dispersed phase volume fraction, the equilibrium time increases. This is because the larger the content of oil phase, the more oil phase needs to be emulsified, and thus the emulsification time increases. It can be found from **Figure 2(b)** that at t=80 min, the Sauter mean diameter d_{32} reaches a stable value. Therefore, when examining the influence of other variables on the Sauter mean diameter d_{32}, the emulsification time is set to 80 min.

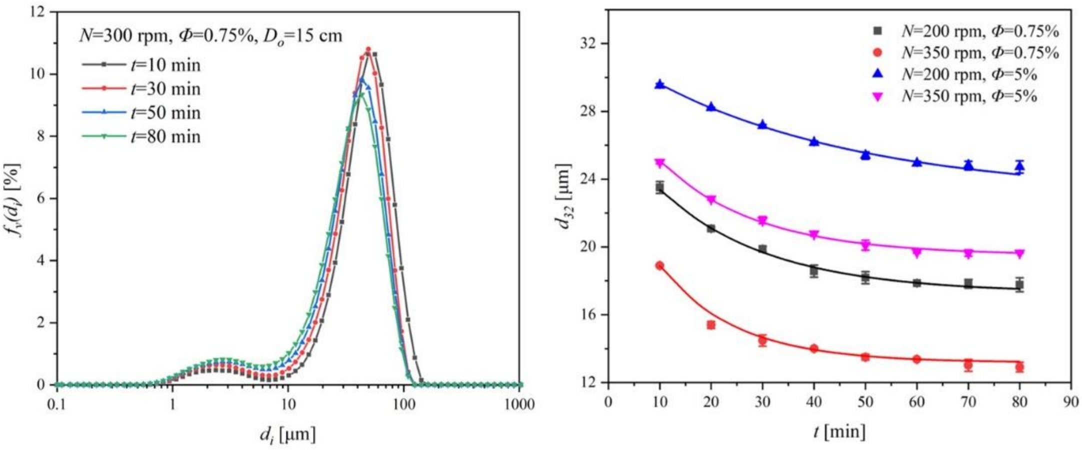

(a) (b)

Figure. 2. Effect of emulsification time on (a) the droplet diameter distribution and (b) Sauter mean diameter d_{32}

4.1.2 Effect of rotational speed

Figure 3(a) shows the effect of rotational speed on droplet size distribution. The changes of D_{10}, D_{50} and D_{90} values in the volume distribution with rotational speed are shown in **supplementary material Table 2S**. With the increase of rotational speed, the DSD shifts to the direction of the smaller diameter peak. **Figure 3(b)** shows the effects of the rotational speed on the Sauter mean diameter d_{32} in the RSFST. With the increase of rotational speed, greater centrifugal force and shear force are generated in RSFST, more energy is input per unit time, energy dissipation rate and shear rate increase, resulting in the decrease of d_{32}. In addition, it can also be found from Figure 3(b) that, within the given dispersed phase volume fraction range, the higher the rotation speed, the smaller the d32, but the decrease percentage is different. At a fixed dispersed phase volume fraction Φ=0.75%, d_{32} decreases from 18.19 μm at 200 rpm to 12.91 μm at 350 rpm, a decrease of 29%. At a fixed dispersed phase volume fraction Φ=5%, d_{32} decreases from 24.72 μm at 200 rpm to 19.65μm at 350 rpm, a decrease of 21%. Where the smaller the dispersed phase volume fraction, the greater the decrease percentage. This is because the smaller the dispersed phase volume fraction, the greater the energy obtained per unit oil phase, and therefore the greater the influence of rotating speed on it. For distilled water as the continuous phase, the Kolmogorov length scale η_k is calculated to be on the order of 10.8−17 μm based on **Eq. (1)**, corresponding to the rotational speed of 200−350 rpm. Applying Kolmogorov-Hinze theory, the droplet breakup is mainly affected by inertial stress as the majority of drop sizes are greater than the η_k[32].

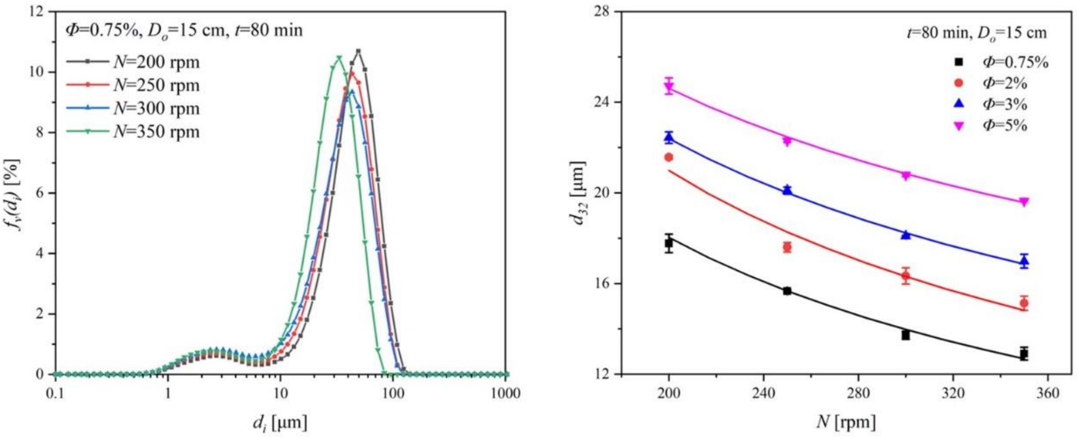

(a) (b)

Figure. 3. Effect of rotation speed on (a) the droplet size distribution and (b) Sauter mean diameter d_{32}

4.1.3 Effect of dispersed phase volume fraction

The effect of different dispersed phase volume fraction on the droplet diameter distribution is investigated and the results are detailed in **Figure 4(a)**. The changes of D_{10}, D_{50} and D_{90} values in the volume distribution with dispersed phase volume fraction are shown in **supplementary material Table 3S**. As the dispersed phase volume fraction increases, the DSD shifts towards the larger droplet size, the liquid-liquid two-phase fragmentation becomes increasingly difficult, and the peaks of the smaller droplet size are very faint and largely overlap. **Figure 4(b)** indicates that Sauter mean diameter d_{32} increases as Φ increases, which is consistent with the results of literature[1]. The reasons are twofold: 1) as the dispersed phase volume fraction increases, the energy per unit time given per unit mass of dispersed phase through the foam filler subsequently decreases, resulting in an increase in Sauter mean diameter d_{32}. 2) The Sauter mean diameter d_{32} increases as dispersed phase volume fraction increases may be attributed to the turbulence dampening[40]. As the dispersed phase volume fraction increases, the turbulence intensity of the continuous phase fluid decays, and some smaller-scale turbulent vortices containing lower energy disappear, resulting in a weakening of their droplet-breaking effect, and the droplets cannot be further broken and can only move with the larger-scale turbulent vortices, with the result that the droplet diameter of the emulsion increases. Therefore, the increase of the dispersed phase volume fraction dampens the turbulent eddies, leaving the η_k much larger than the droplet diameters. As a result, weakening of its droplet breaking effect and the droplet cannot be broken further[41].

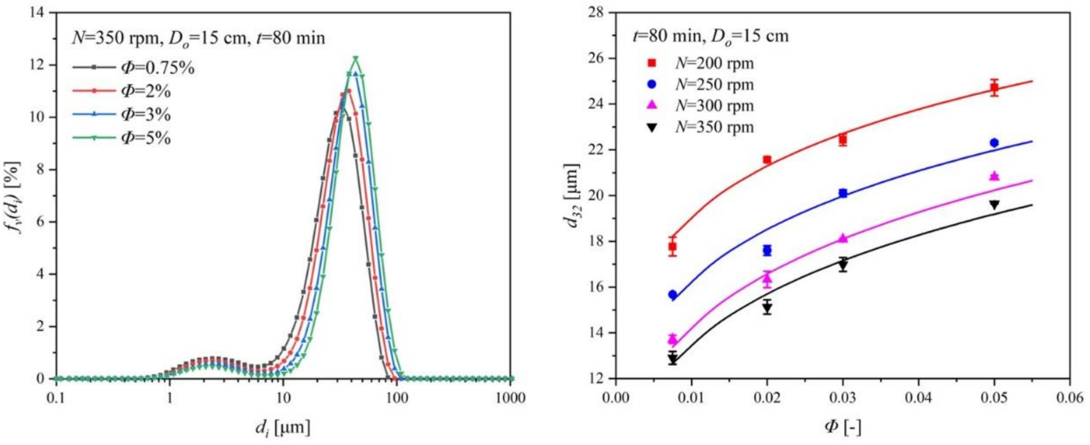

(a) (b)

Figure. 4. Effect of dispersed phase volume fraction on (a) the droplet size distribution and (b) Sauter mean diameter d_{32}

4.1.4 Effect of continuous-phase viscosity

The effect of different continuous phase viscosities on the droplet diameter distribution was investigated and the results are detailed in **Figure 5(a)**. The changes of D_{10}, D_{50} and D_{90} values in the volume distribution with continuous phase viscosity are shown in **supplementary material Table 4S**. The results show that as the continuous-phase viscosity increases, the DSD shifts first towards the small droplet diameter and then towards the large droplet diameter. The volume percentage of small droplet size increases with the increase of continuous phase viscosity. According to the Kolmogorov-Hinze theory, the increase of continuous phase viscosity leads to the increase of the length scale of the smallest eddies η_k. Therefore, the average diameter of droplets is close to or less than η_k, and viscous stress plays an important role in droplet breakage. As the role of viscous stress in the fragmentation process of droplets becomes more significant, it results in an increase in the volume percentage of the small drop size [1]. In addition, it can be seen from **Figure 5(b)** that with the increase of continuous phase viscosity, the Sauter mean diameter d_{32} first decreases and then increases. The dynamic equilibrium is mainly affected by the coalescence frequency because of relatively smaller droplet sizes present. The slope values m of the power number curve is positive. Therefore, the coalescence frequency given by **Eq. (10)** decreases with increasing μ_c, resulting in the decrease of d_{32}. Li et al.[42] showed that the droplet diameter is proportional to the ratio of surface tension to density of the liquid. Adding glycerol to distilled water can not only adjust the viscosity of the continuous phase, but also slightly reduce the interfacial tension and increase the density of the continuous phase (see Table 1). Therefore, with the increase of continuous phase viscosity, the Sauter mean diameter d_{32} decreases. With the further increase of the μ_c, the breakage rate given by **Eq. (9)** finally decreases faster than the coalescence rate with the result that d_{32} reaches a minimum and then starts increasing, which is consistent with the results obtained by Stamatoudis et al [30].

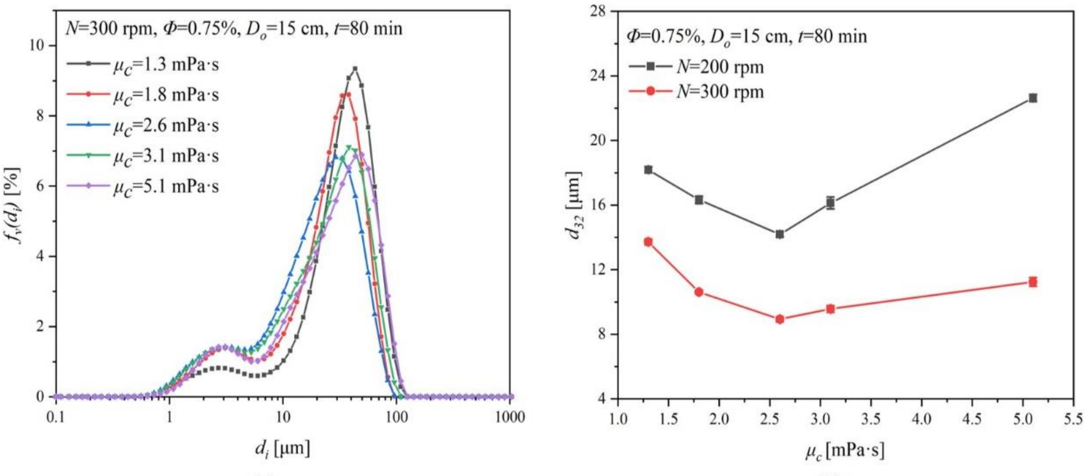

(a) (b)

Figure. 5. Effect of continuous-phase viscosity on (a) the droplet size distribution and (b) Sauter mean diameter d_{32}

4.1.5 Effect of packing size

The effect of different packing size on droplet diameter distribution was investigated and the results are detailed in **Figure 6(a)**. The changes of D_{10}, D_{50} and D_{90} values in the volume distribution with packing size are shown in **supplementary material Table 5S**. The results show that as the packing size increases, the DSD shifts towards smaller droplet sizes and the droplet diameter distribution becomes narrower. And shown in **Figure 6(b)**, the Sauter mean diameter d_{32} also decreases as the packing size increases. With the increase of packing size, the generated centrifugal force and average energy dissipation rate increase with the increase of radius. Therefore, the shear rate is expected to increase with a higher packing diameter, resulting in the reduction of the Sauter mean diameter d_{32}.

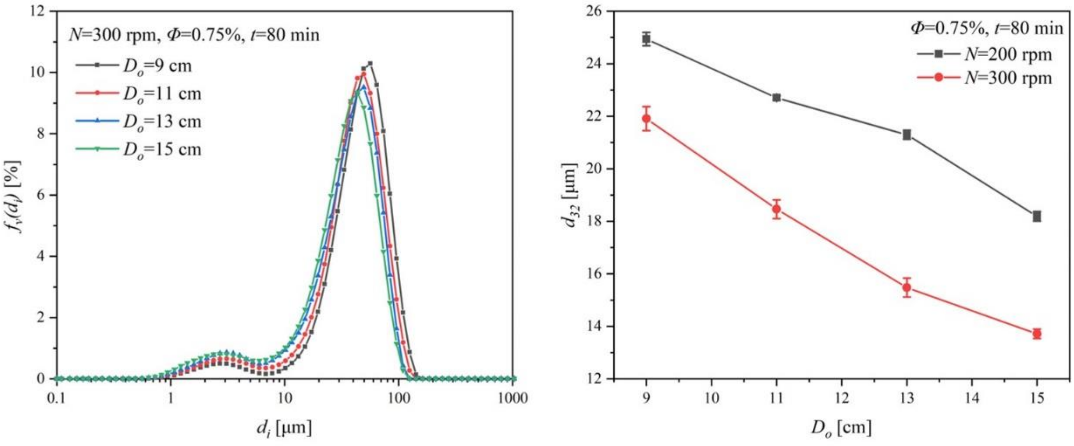

(a) (b)

Figure. 6. Effect of packing size on (a) the droplet size distribution and (b) Sauter mean diameter d_{32}

4.1.5 Compared with the Rushton stirrer

Figure 7 shows the comparison of emulsion efficiency between RSFST and RT stirrer with dispersed phase volume fraction of 0.75% and 5%. With the increase of emulsification time and energy dissipation rate, the Sauter mean diameter d_{32} decreases gradually. At a fixed dispersed phase volume fraction Φ=0.75%, for a relatively low energy dissipation rate (ε_{avg}= 0.296 W/kg for RT and ε_{avg}= 0.287 W/kg for RSFST), the Sauter mean diameter d_{32} of the emulsion produced by the RSFST and RT stirrer was 17.53 μm and 19.68 μm, respectively; for relatively high energy dissipation rate (ε_{avg}= 0.679 W/kg for RT and ε_{avg}= 0.658 W/kg for RSFST), the Sauter mean diameter d_{32} of the emulsion produced by the RSFST and RT stirrer was 15.68 μm and 17.73 μm, respectively. With a fixed energy input, smaller droplet size can be generated with RSFST compared to a RT. **Figure 7(c-d)** shows the comparison of droplet size distribution between RSFST and RT stirrer with dispersed phase volume fraction of 0.75% and 5%, respectively. With a fixed energy input, the RSFST droplet size distribution becomes narrower and shifts toward smaller droplet diameters compared to RT. This is a direct proof that RSFST shows a superior emulsion efficiency.

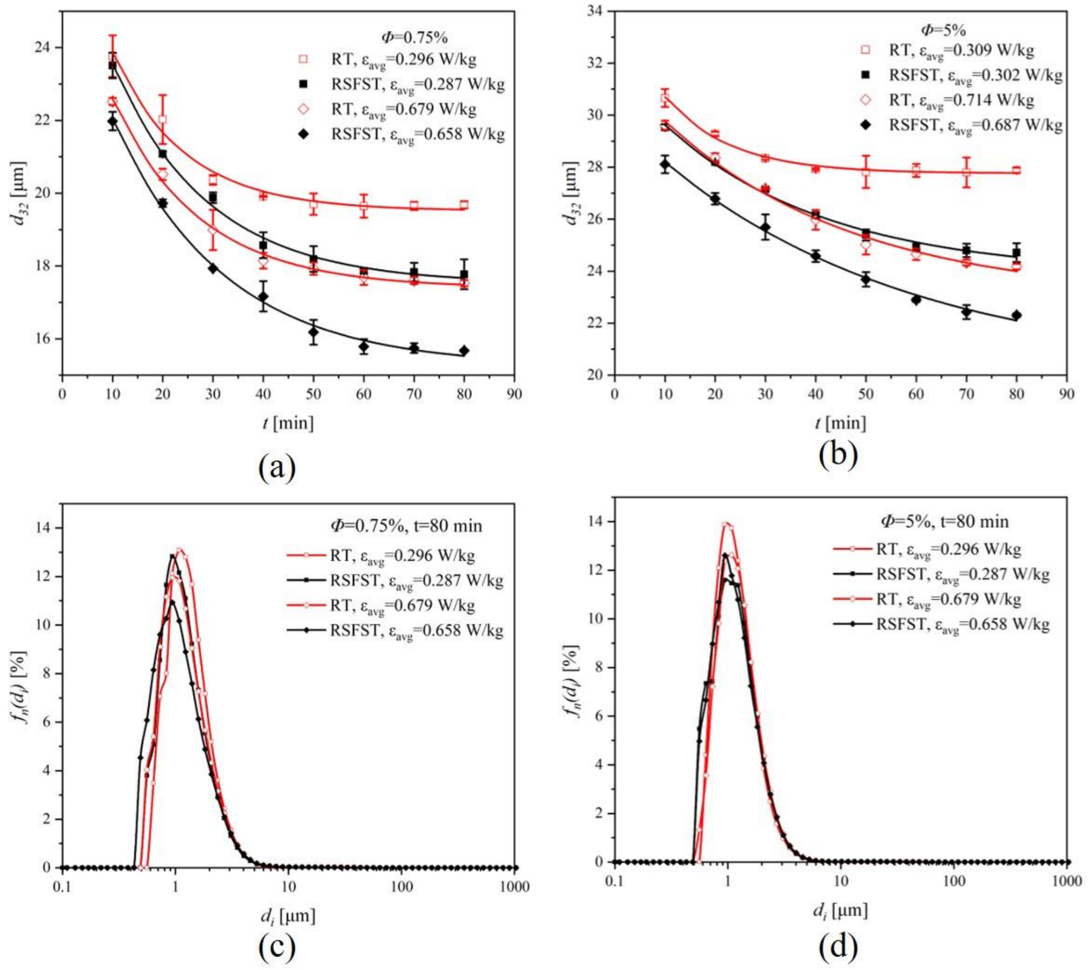

Figure. 7. Comparison between Sauter mean diameter d_{32} and droplet size distribution of RSFST and RT stirrer at Φ=0.75% and 5%

4.2 Droplet diameter distribution modelling

According to **Eq. (13)**, the number DSD converted from the corresponding bimodal volume DSD shows an obvious unimodal distribution under the smaller droplet diameter (< 1 μm) (see **Figure 8**). In this study, Frechet distribution **(Eq. 14)** is used to describe the experimental data.

The normal distribution function, log-normal distribution function and Frechet distribution function were used to fit the experimental data for comparison. See **supplementary material Figure 1S** for the comparison of droplet size distribution models at other rotation speeds. From **Figure 8** normal distribution fails to describe the experimental date while the log-normal distribution function can describe the distribution trend of the but with a noticeable deviation in the peak and peak width. The Frechet distribution function fits the experimental data. The mean and standard deviation of the Frechet distribution in **Figure 8 (a)** are 1.513 and 0.83 respectively, and the mean and standard deviation of the Frechet distribution in **Figure 8 (b)** are 1.476 and 1.128 respectively. As shown by the droplet size distribution, a series of smaller droplets (< 3 μm) were found in the experiment. The volume frequency of smaller droplets is low, but the corresponding number frequency is quite high, resulting in a spike in the number frequency curve. Since Frechet distribution function is one of the extreme value probability functions, the best fitting can be obtained[36].

In previous research, Ramkrishna and colleagues [43] reported the self-similar breakup of droplet turbulence in stirred vessel. Wang and Calabrese [44] alternatively scaled droplet size using Sauter mean diameter and found that scaled size distributions for different operating conditions of col-lapsed onto one single curve. In this work, we use similar scaled variables to test self-similar evolution. **Supplementary material**

Figure 2S shows the scaled size distribution for different operating conditions. These figures show that the scaled size distribution falls on a curve, which confirms that the droplet breakup in the current system occurs in a self-similar manner and that the width of the scaled size distribution is independent of the operating conditions.

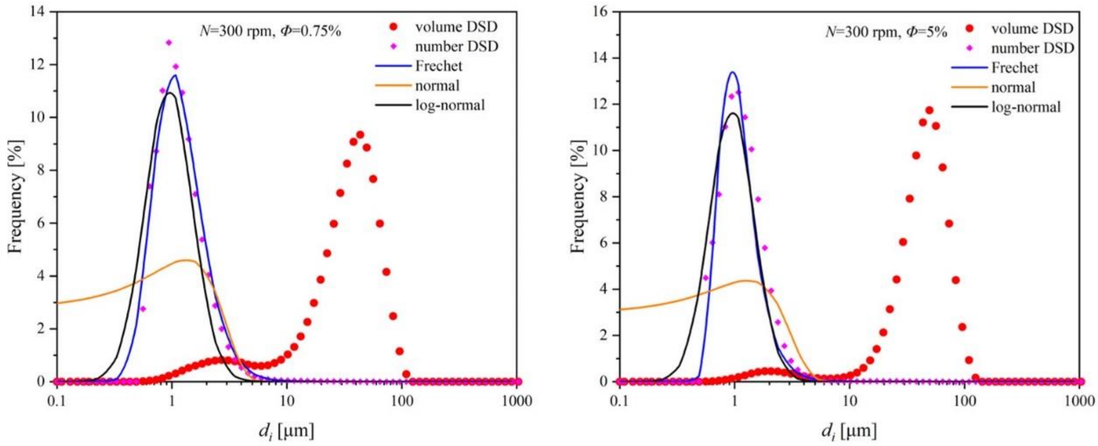

(a) (b)

Figure. 8. Comparison of experimental results ((a) and (b)) with the distribution function of normal, log-normal, and Frechet

4.3 Relation for Sauter Mean Diameter d_{32}

4.3.1 Proportional relationship between d_{32} and d_{max}

In a practical sense, the proportionality constant between d_{32} and d_{max} is of importance[36]. Under the various operating conditions in this study, the relationship between d_{32} and d_{max} is shown in **Figure 9**, where d_{max} is represented by d_{v95} (droplet diameter with cumulative volume fraction of 95%). Based on **Eq. (4)**, the constant C_2 can be determined as 0.24 (The d_{32} and d_{max} are well fitted within a deviation of ±5%, where R^2 is 0.896.), by fitting a linear relationship in **Figure 9**. It should be noted this value is different from the results of other studies. The proportionality constant of d_{32} and d_{max} reported by Sprow[24], Brown and Pitt[45] and Calabrese et al.[44] are 0.38, 0.70 and 0.48-0.6 respectively. This difference is due to the polydispersity of the size distribution as a result of the peaks appearing at smaller particle sizes (<3 μm). The contribution of smaller droplets is particularly important in the size distribution in number, because it directly affects the phase interface area of the dispersed phase. According to the definition of d_{32} (see **Eq. (6)**), the increase of the interface area of dispersed phase will lead to the decrease of d_{32} and the proportional constant will decrease.

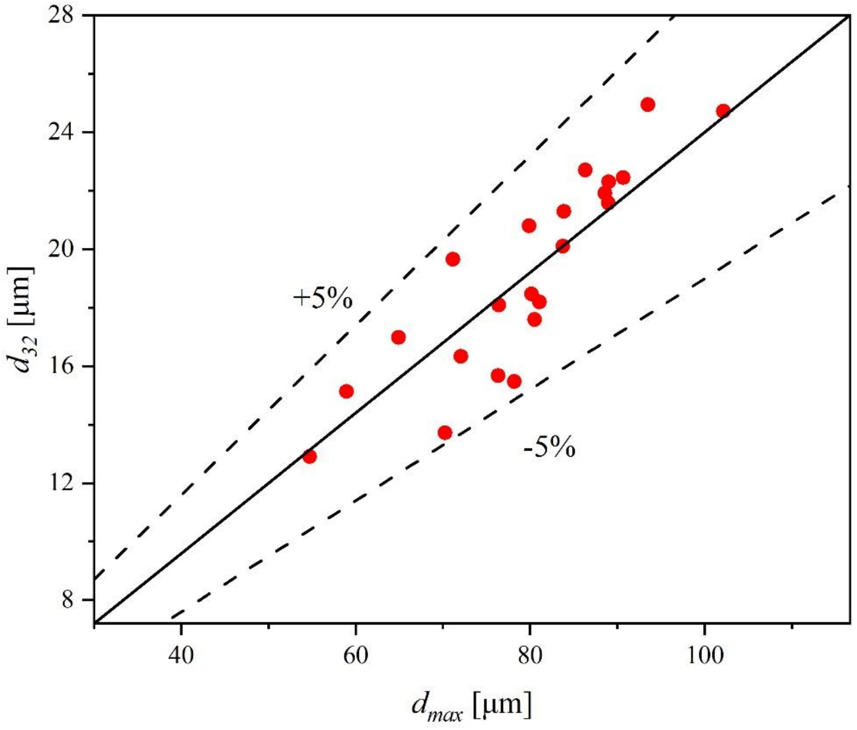

Figure. 9. Variation of d_{32} with d_{max}

4.3.2 Correlation for d_{32}

Based on **Eq. (8)**, the dispersed phase volume fraction is considered to have an important effect on the droplet size. Correlating the experimentally measured Sauter mean diameter d_{32} with dispersed phase volume fraction Φ and the Weber number We, **Eq. (19)** was obtained with a correlation coefficient of $R^2 = 0.94$.

$$\frac{d_{32}}{D} = 0.018(1 + 10.49\Phi)We^{-0.6} \tag{19}$$

The value of C_5 is 10.49 and values of C_5 in the literature range from 0.5 to 20[1]. It indicates a relatively low coalescence tendency. **Figure 10** shows the correlation of the Sauter mean diameter with the dispersed phase volume fraction and the Weber number. A correlation within ±20% deviation is proposed to predict the Sauter mean diameter d_{32} based on the Weber number and dispersed phase volume fraction. The correlation is developed for RSFST. The results show that the prediction model of Sauter mean diameter established by combining the mechanistic models and experimental results is in good agreement with our data.

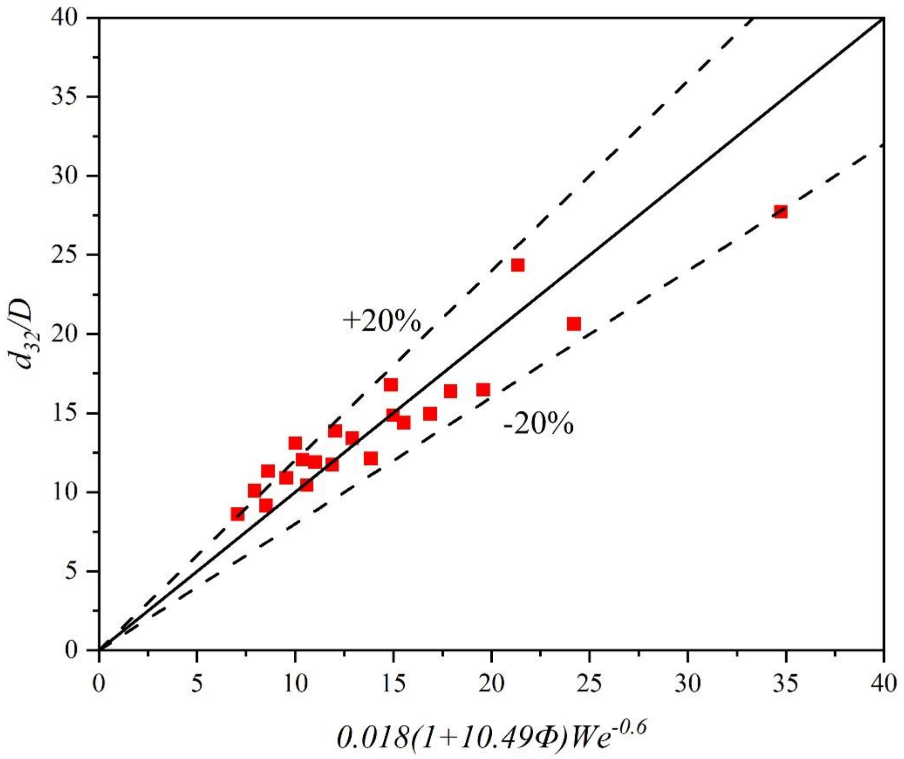

Figure. 10. Correlation of d_{32} with dispersed phase volume fraction and Weber number

5. Conclusion

In this work, the emulsion process of kerosene-water is studied in an RSFST. The effect of varying rotational speed, dispersed phase volume fraction, continuous phase viscosity and packing size on the Sauter mean diameter d_{32} and droplet size distribution in RSFST is investigated. The results show that the droplet volume distribution is bimodal for all emulsification conditions with a smaller (or secondary) peak appearing at around 3 μm. The Sauter mean diameter d_{32} decreases with increasing rotational speed and packing size and increases with increasing dispersed phase volume fraction. The Sauter mean diameter d_{32} decreases first and then increases with increasing continuous phase viscosity. With a bimodal distribution of the droplet volume, the linear relationship between the Sauter mean diameter d_{32} and the maximum stable droplet diameter d_{max} is still valid, but its proportionality constant is smaller than that of the single-peaked distribution. With a given energy input, a smaller droplet size can be generated in RSFST compared to a RT, indicating a superior emulsifications performance of RSFST. In contrast to normal and lognormal functions, the Frechet function can describe single-peaked number DSD very well. A correlation within ±20% deviation is proposed to predict the Sauter mean diameter d_{32} based on the Weber number and dispersed phase volume fraction.

Associated Content

Supporting Information

Effect of operating parameters and physical parameters on the D_{10}, D_{50} and D_{90} values; comparison of droplet size distribution models at other rotation speeds; cumulative droplet size distribution and the self-similar behavior under different physical and operating conditions

Author Information

Corresponding Author

Yu-Cheng Yang — *Department of Chemical and Pharmaceutical Engineering, School of Chemical Engineering, Huaqiao University, Fujian 361021, China;* **Tel:** +86-0592-6162300; **Fax:** +86-0592-6162300; **Email:** yangyc@hqu.edu.cn

Author

Ze-Teng Wang — *Department of Chemical and Pharmaceutical Engineering, School of Chemical Engineering, Huaqiao University, Fujian 361021, China*

Si-Xing Chen — *Department of Chemical and Pharmaceutical Engineering, School of Chemical Engineering, Huaqiao University, Fujian 361021, China*

Yi Ouyang — *Laboratory for Chemical Technology, Ghent University, Gent 125, 9052, Belgium*

Xue-Qin Zhang — *Department of Chemical and Pharmaceutical Engineering, School of Chemical Engineering, Huaqiao University, Fujian 361021, China*

Bing-De Zheng — *Department of Chemical and Pharmaceutical Engineering, School of Chemical Engineering, Huaqiao University, Fujian 361021, China*

Na Zhang — *Department of Chemical and Pharmaceutical Engineering, School of Chemical Engineering, Huaqiao University, Fujian 361021, China*

Jing Ye — *Department of Chemical and Pharmaceutical Engineering, School of Chemical Engineering, Huaqiao University, Fujian 361021, China*

Mei-Tian Xiao — *Department of Chemical and Pharmaceutical Engineering, School of Chemical Engineering, Huaqiao University, Fujian 361021, China*

Acknowledgments

This work was supported by the National Nature Science Foundation of China [No. 22278166], External Cooperation Program of Science and Technology Planning of Fujian Province [No. 2021I0016], and Promotion Program for Young and Middle-Aged Teacher in Science and Technology Research of Huaqiao University [No. ZQN-714]. The authors thank Instrumental Analysis Center of Huaqiao University for analysis support.

Nomenclature

d_{32}	Sauter mean diameter [m]
d_{max}	maximum stable droplet diameter [m]
d_{95}	Droplet diameter with cumulative volume fraction of 95% [m]
D	impeller diameter [m]
C_1-C_9	constant [-]
N	rotation speed [rpm]
d_i	the *i*th droplet diameter [m]
$f_n(d_i)$	frequency by number of the droplets of the *i*th diameter [%]
$f_v(d_i)$	frequency by volume of the droplets of the *i*th diameter [%]
$\bar{d}_i$	mean diameter in the normal distribution [m]
$\overline{ln\,(d_i)}$	mean in the log-normal distribution [m]

$P_v(d_i)$	probability by volume of droplets of ith size [%]
$P_n(d_i)$	probability by number of droplets of ith size [%]
h	height of the rotating solid foam stirrer [m]
D_i	inner diameter of the rotating solid foam stirrer [m]
D_o	outer diameter of the rotating solid foam stirrer [m]
T	inner diameter of the tank [m]
H	height of the tank [m]
C	distance between the bottom of the foam filler and the tank bottom [m]
C'	distance between the bottom of the Rushton and the tank bottom [m]
D'	diameter of the Rushton [m]
P_{in}	power consumption [W]
M	torque [N·m]
M_n	torque of the bearing loss correction [N·m]
V_H	working liquid volumes [m^3]
$N(t)$	total number of droplets at time t per unit dispersion volume
$A'(d)$	the fraction of droplets with diameter d
m	the slope of the log-log plot of impeller power vs. impeller Reynold's number

a	the interface area per unit volume [1/m]

Greek symbols

ρ_c	density of the continuous phase [kg/m^3]
σ	interfacial tension [N·m]
Φ	dispersed phase volume fraction [-]
σ_d	standard deviation of the normal distribution [m]
$\sigma_{ln(d)}$	standard deviation of the log-normal distribution [m]
μ_c	viscosity of the continuous phase [Pa·s]
μ_d	viscosity of the dispersed phase [Pa·s]
ρ_d	density of the dispersed phase [kg/m^3]
ε_{avg}	average energy dissipation rate per unit mass of fluid [W/kg]
ε	energy dissipation rate per unit mass of fluid [W/kg]
v_c	the kinematic viscosity of the continuous phase [m^2/s]
η_k	Kolmogorov length scale [m]
α	parameter in the Fréchet probability density function [-]
β	parameter in the Fréchet probability density function [-]

Dimensionless numbers

We	Weber number, $\frac{\rho_c N^2 D^3}{\sigma}$

Abbreviations

RSFST	Rotating solid foam stirrer tank
RT	Rushton
DSD	Droplet size distribution
Gly#w	Glycerinated water

References

(1) Shi, J.; Xu, S.; Qin, H.; Liu, Y.; Li, W.; Zhang, J. Single-Pass Emulsification Processes in Two Different Inline High Shear Mixers. *Ind. Eng. Chem. Res.* **2013**, *52* (40), 14463-14471.

(2) Lv, G.; Wu, L.; Wang, X.; Liao, L.; Li, Z.; He, W. Regeneration of Caramel Saturated Activated Carbon jointly by Microwave and Extractive Method. *Int. J. Chem. React* **2012**, *10*, 2059-2063.

(3) Li, Y.; Ye, H.; Han, K.; Liu, H. Progress in intensification for mixing process and equipment. *Chem. Ind. Eng. Prog.* **2010**, *29* (04), 593-599.

(4) Zhou, G.; Kresta, S. M. Correlation of mean drop size and minimum drop size with the turbulence energy dissipation and the flow in an agitated tank. *Chem. Eng. Sci.* **1998**, *53* (11), 2063-2079.

(5) Stankiewicz, A. I.; Moulijn, J. A. Process Intensification: Transforming Chemical Engineering. *CHEM ENG PROG* **2000**, *96* (1), 22-34.

(6) Urban, K.; Wagner, G.; Schaffner, D.; Roglin, D.; Ulrich, J. Rotor-stator and disc systems for emulsification processes. *Chem Eng Technol* **2006**, *29* (1), 24-31.

(7) Zhang, J.; Xu, S.; Li, W. High shear mixers: A review of typical applications and studies on power draw, flow pattern, energy dissipation and transfer properties. *Chem Eng Process* **2012**, *57-58*, 25-41.

(8) Maindarkar, S. N.; Hoogland, H.; Henson, M. A. Predicting the combined effects of oil and surfactant concentrations on the drop size distributions of homogenized emulsions. *Colloids Surf* **2015**, *467*, 18-30.

(9) O'Sullivan, J.; Murray, B.; Flynn, C.; Norton, I. Comparison of batch and continuous ultrasonic emulsification processes. *J Food Eng* **2015**, *167*, 114-121.

(10) Yang, Y.; Yang, S.; Arowo, M. Research progress in a rotating foam reactor. *Chem.*

Ind. Eng. Prog. **2018**, *37* (6), 2046-2052.

(11) Tschentscher, R.; Nijhuis, T. A.; John, V. D. R. S.; Schouten, J. C. Glucose oxidation in slurry reactors and rotating foam reactors. *Ind. Eng. Chem. Res.* **2012**, *51* (4), 1620-1634.

(12) Lali, F.; Boettcher, G.; Schoeneich, P. M.; Haase, S.; Hempel, S.; Lange, R. Preparation and characterization of Pd/Al2O3 catalysts on aluminum foam supports for multiphase hydrogenation reactions in rotating foam reactors. *Chem Eng Res Des* **2015**, *94*, 365-374.

(13) Yang, Y.; Zeng, S.; Ouyang, Y.; Sang, L.; Yang, S.; Zhang, X.; Huang, Y.; Ye, J.; Xiao, M.; Zhang, N. An intensified ozonation system in a tank reactor with foam block stirrer: Synthetic textile wastewater treatment and mass transfer modeling - ScienceDirect. *Sep. Purif. Technol* **2020**, *257*, 117909 - 117909.

(14) Wang, Z.; Yang, Y.; Zeng, S.; Arowo, M.; Zhang, X.; Zheng, B.; Zhang, N.; Ye, J.; Xiao, M. Treatment of organic wastewater by ozone in a continuous rotating solid foam stirrer tank. *Chem Eng Process* **2022**, *174*, 108866 - 108866.

(15) Yang, Y.; Yu, X.; Yu, Q.; Yang, S.; Arowo, M. Micromixing Efficiency in a Multiphase Reactor with a Foam Block Stirrer. *Can J Chem Eng* **2018**, *97*, 1560-1567.

(16) Tschentscher, R.; Spijkers, R. J. P.; Nijhuis, T. A.; Van Der Schaaf, J.; Schouten, J. C. Liquid− solid mass transfer in agitated slurry reactors and rotating solid foam reactors. *Ind. Eng. Chem. Res.* **2010**, *49* (21), 10758-10766.

(17) Ghotli, R. A.; Abbasi, M. R.; Bagheri, A.; Raman, A. A. A.; Ibrahim, S.; Bostanci, H. Experimental and modeling evaluation of droplet size in immiscible liquid-liquid stirred vessel using various impeller designs. *J TAIWAN INST CHEM E* **2019**, *100*, 26-36.

(18) De Hert, S. C.; Rodgers, T. L. On the effect of dispersed phase viscosity and mean residence time on the droplet size distribution for high-shear mixers. *Chem. Eng. Sci.* **2017**, *172*, 423-433.

(19) Kolmogorov, A. N. The Local Structure of Turbulence in Incompressible Viscous Fluid for Very Large Reynolds Numbers. *Proc. Math. Phys. Eng. Sci* **1991**, *434* (1890), 9-13.

(20) Kichatov, B. V.; Korshunov, A. M.; Boiko, I. V.; Assorova, P. V. Effect of impeller blade geometry on drop size in stirring of immiscible liquids. *Theor* **2003**, *37* (1), 19-24.

(21) Pacek, A. W.; Chamsart, S.; Nienow, A. W.; Bakker, A. The influence of impeller type on mean drop size and drop size distribution in an agitated vessel. *Chem. Eng. Sci.* **1999**, *54* (19), 4211-4222.

(22) Nienow, A. W. Break-up, coalescence and catastrophic phase inversion in turbulent contactors. *Adv. Colloid Interface Sci* **2004**, *108*, 95-103.

(23) El-Hamouz, A. Drop Size Distribution in a Standard Twin-Impeller Batch Mixer at High Dispersed-Phase Volume Fraction. *Chem Eng Technol* **2009**, *32* (8), 1203-1210.

(24) Sprow, F. B. Distribution of drop sizes produced in turbulent liquid—liquid dispersion. *Chem. Eng. Sci.* **1967**, *22* (3), 435-442.

(25) Nishikawa, M.; Mori, F.; Kayama, T.; Nishioka, S. Drop Size Distribution in a Liquid-Liquid Phase Mixing Vessel. *J CHEM ENG JPN* **2006**, *24* (1), 88-94.

(26) Li, M.; Liu, C.; Liang, C.; Liu, C.; Li, J. Study of Bimodal Drop Size Distributions of Emulsion. *J DISPER SCI TECHNOL* **2014**, *35* (3), 397-402.

(27) Desnoyer, C.; Masbernat, O.; Gourdon, C. Experimental study of drop size distributions at high phase ratio in liquid-liquid dispersions. *Chem. Eng. Sci.* **2003**, *58* (7), 1353-1363.

(28) Ghotli, R. A.; Abbasi, M. R.; Bagheri, A.; Raman, A. A. A.; Ibrahim, S.; Bostanci, H. Experimental and modeling evaluation of droplet size in immiscible liquid-liquid stirred vessel using various impeller designs. *Journal of the Taiwan Institute of Chemical Engineers* **2019**, *100*, 26-36.

(29) Kraume, M.; Gabler, A.; Schulze, K. Influence of physical properties on drop size distributions of stirred liquid-liquid dispersions. *Chem Eng Technol* **2004**, *27* (3), 330-334.

(30) Stamatoudis, M.; Tavlarides, L. L. Effect of continuous-phase viscosity on the drop sizes of liquid-liquid dispersions in agitated vessels. *Ind. Eng. Chem. Process. Des* **1985**, *24* (4), 1175-1181.

(31) Chen, H.; Middleman, S. Drop size distribution in agitated liquid-liquid systems. *AIChE J* **1967**, *13* (5), 989-995.

(32) Hall, S.; Cooke, M.; El-Hamouz, A.; Kowalski, A. J. Droplet break-up by in-line Silverson rotor-stator mixer. *Chem. Eng. Sci.* **2011**, *66* (10), 2068-2079.

(33) Chatzi, E. G.; Kiparissides, C. Dynamic simulation of bimodal drop size distributions in low-coalescence batch dispersion systems. *Chem. Eng. Sci.* **1992**, *47* (2), 445-456.

(34) Arai, K.; Konno, M.; Matunaga, Y.; Saito, S. Effect of dispersed-phase viscosity on the maximum stable drop size for breakup in turbulent flow. *J CHEM ENG JPN* **2006**, *10* (4), 325-330.

(35) Vankova, N.; Tcholakova, S.; Denkov, N. D.; Ivanov, I. B.; Vulchev, V. D.; Danner, T. Emulsification in turbulent flow 1. Mean and maximum drop diameters in inertial and viscous regimes. *J. Colloid Interface Sci* **2007**, *312* (2), 363-380.

(36) Liu, C.; Li, M.; Liang, C.; Wang, W. Measurement and analysis of bimodal drop size distribution in a rotor–stator homogenizer. *Chem. Eng. Sci.* **2013**, *102*, 622-631.

(37) Weiss, J.; McClements, D. J. Mass transport phenomena in oil-in-water emulsions containing surfactant micelles: Solubilization. *Langmuir* **2000**, *16* (14), 5879-5883.

(38) Manzano Martínez, A. N.; Assirelli, M.; van der Schaaf, J. Droplet size and liquid-liquid mass transfer with reaction in a rotor-stator Spinning Disk Reactor. *Chem. Eng. Sci.* **2021**, *242*.

(39) El-Hamouz, A.; Cooke, M.; Kowalski, A.; Sharratt, P. Dispersion of silicone oil in water surfactant solution: Effect of impeller speed, oil viscosity and addition point on drop size distribution. *Chem Eng Process* **2009**, *48* (2), 633-642.

(40) Shi, J. T.; Xu, S. Q.; Qin, H. Y.; Liu, Y. L.; Li, W.; Zhang, J. L. Single-Pass Emulsification Processes in Two Different Inline High Shear Mixers. *Industrial & Engineering Chemistry Research* **2013**, *52* (40), 14463-14471.

(41) Cohen; Ruben, D. Effect of turbulence damping on the steady-state drop size distribution in stirred liquid-liquid dispersions. *Ind. Eng. Chem. Res.* **1991**, *30* (1), 277-279. Angle, C. W.; Hamza, H. A. Drop sizes during turbulent mixing of toluene-heavy

oil fractions in water. *AIChE J* **2006**, *52* (7), 2639-2650.

(42) Li, Y.; Wang, S.; Sun, B.; Arowo, M.; Zou, H.; Chen, J.; Shao, L. Visual study of liquid flow in a rotor-stator reactor. *Chem. Eng. Sci.* **2015**, *134*, 521-530.

(43) Ganesan; Narsimhan; Doraiswami; Ramkrishna; Gupta, J. P. Analysis of drop size distributions in lean liquid-liquid dispersions. *AIChE J* **1980**, *26* (6), 991–1000.

(44) Wang, C.; Calabrese, R. V. Drop breakup in turbulent stirred-tank contactors. Part II: Relative influence of viscosity and interfacial tension. *AIChE J* **1986**, *32* (4), 667–676.

(45) Brown, D. E.; Pitt, K. Drop size distribution of stirred non-coalescing liquid—liquid system. *Chem. Eng. Sci.* **1972**, *27* (3), 577-583.

Declaration of Competing Interest

The authors declare that they have no known competing financial interests or personal relationships that could have appeared to influence the work reported in this paper.

Table of Contents graphic